Journal of CO2 Utilization 52 (2021) 101679

Contents lists available at ScienceDirect

Journal of CO2 Utilization

journal homepage: www.elsevier.com/locate/jcou

Electrochemically driven efficient enzymatic conversion of CO_2 to formic acid with artificial cofactors

Zhibo Zhang [a], Tudor Vasiliu [b], Fangfang Li [a], Aatto Laaksonen [a,b,c,d], Francesca Mocci [e,*], Xiaoyan Ji [a,*]

[a] Energy Engineering, Division of Energy Science, Luleå University of Technology, 97187, Luleå, Sweden
[b] Centre of Advanced Research in Bionanoconjugates and Biopolymers, Romanian Academy Petru Poni (PP) Institute of Macromolecular Chemistry, 00487, Iasi, Romania
[c] Department of Materials and Environmental Chemistry, Arrhenius Laboratory, Stockholm University, SE-106 91, Stockholm, Sweden
[d] State Key Laboratory of Materials-Oriented and Chemical Engineering, Nanjing Tech University, Nanjing, 210009, PR China
[e] Dipartimento di Scienze Chimiche e Geologiche, Università degli Studi di Cagliari, 09042 Cagliari, Italy

ARTICLE INFO

Keywords:
CO_2 conversion
Formic acid
Enzyme
Artificial cofactors
Electrocatalysis
Umbrella sampling
Molecular dynamics

ABSTRACT

Enzymatic reduction of CO_2 to formic acid with the enzyme formate dehydrogenase (FDH) and a cofactor is a promising method for CO_2 conversion and utilization. However, the natural cofactor nicotinamide adenine dinucleotide (NADH) shows some drawbacks such as a low reduction efficiency and forms isomers or dimers (1,6 - NADH or NAD dimer) in the regeneration reaction. To overcome them and to improve the production of formic acid, in this work, the artificial cofactors, i.e., the bipyridinium-based salts of methyl viologen (MV^{2+}), 1,1'-dicarboxymethyl-4,4'-bipyridinium bromine (DC^{2+}), and 1,1'-diaminoethyl-4,4'-bipyridinium bromine (DA^{2+}), were used to replace NADH, and the effect of different functional groups on the electrochemical regeneration and catalytic performance in the enzymatic reaction was studied systematically. Also, studies using the natural cofactor NADH were carried out for comparison. It was found that the cofactor with amino groups showed the highest catalytic efficiency (k_{cat}/K_m) of 0.161 $mM^{-1}min^{-1}$, which is 536 times higher than that of the natural cofactor NADH. Molecular Dynamics simulations were conducted to give further molecular insight into the behavior of the cofactors. Analyzing the free energy profiles of the complexes between CO_2 in the FDH active site with different artificial cofactors indicated that the artificial cofactor with the amino groups had the highest affinity for CO_2, being consistent with the experimental observations.

1. Introduction

The reduction of CO_2 to value-added fuels and chemicals to both alleviate the greenhouse effect and promote resource utilization has attracted great interest from researchers [1–2]. Formic acid (carbonaceous fuel), an important chemical feedstock and hydrogen storage material in industries [3], can be produced via chemical [4], photocatalytic [5], electrochemical [6], and enzymatic [7] conversion of CO_2. However, chemical conversion normally takes place under harsh conditions using expensive metal catalysts and leads regularly to high energy demand and capitalized costs [8]. Photocatalytic conversion is complex and unstable, while the reaction process of electrochemical conversion using a metal-based catalyst is difficult to control, and byproducts are often generated. Enzymatic conversion of CO_2, in turn, is a promising method to produce formic acid with high selectivity and low energy usage due to the high specificity and activity of the enzyme under mild conditions [9–10].

Much research has been conducted to investigate the enzymatic conversion of CO_2 to formic acid. It is well known that, in the biological metabolism (i.e., Calvin cycle), formate dehydrogenase (FDH) serves as the catalysts to oxidize formic acid to CO_2 with the redox cofactor NAD^+ (i.e., the reverse reaction of Equation 1) [11]. Inspired by this, FDH is used in CO_2 reduction to formic acid (Equation 1) due to its high selectivity in the formic acid production and nearly without producing any byproducts. For instance, Choe et al. [12] did carry out CO_2 reduction studies using commercial FDH from *Candida boidinii* (CbFDH) with NADH as a cofactor, producing 0.13 mM formate in 120 min without any co-products. However, when NADH is used as the cofactor, the yield of formic acid is low, simply because this reaction is reversible (see

* Corresponding authors.
E-mail addresses: fmocci@unica.it (F. Mocci), xiaoyan.ji@ltu.se (X. Ji).

https://doi.org/10.1016/j.jcou.2021.101679
Received 18 May 2021; Received in revised form 31 July 2021; Accepted 11 August 2021
Available online 19 August 2021

Equation 1) and the oxidation rate of formic acid back to CO_2 is much faster (around 30 times) than the reduction rate of CO_2 to formic acid [13]. Moreover, the amount of the expensive NADH that is needed is equal to the amount of formic acid generated, impeding the potential for any large-scale applications [14]. To address these issues, Zhang et al. [15] investigated the electrocatalytic reduction of NAD^+ to NADH and its coupling with enzymatic conversion of CO_2, suppressing the reverse reaction by consuming NAD^+ (thus enhancing CO_2 conversion) and this way achieving a better NADH regeneration (also cutting down the cost). Similarly, Kuk et al. [16] reported the photoelectrocatalytic reduction of NAD^+ to NADH by integrating it to the enzymatic conversion of CO_2. However, in most developed methods for the NADH regeneration, either some extra byproducts are produced or NAD^+ is reduced to an inactive NAD dimer or 1,6-NADH, which both cannot be used successfully in CO_2 conversion in comparison with NADH [15]. Also the oxidation of formic acid could not be completely eliminated. How to increase the efficiency of formic acid production, overcome the drawbacks of NADH/NAD^+, and improve the electro-recycling stability of cofactor still remains a major challenge for any large-scale enzymatic conversion of CO_2.

$$CO_2 + NADH \overset{FDH}{\rightleftarrows} HCOO^- + NAD^+ \quad (1)$$

$$CO_2 + NADH \overset{FDH}{\rightleftharpoons} HCOO^- + NAD^+ \quad (2)$$

$$CO_2 + 2BP^{+\bullet} + H^+ \overset{FDH}{\not\rightleftharpoons} HCOO^- + 2BP^{2+}$$

Recently, bipyridinium (BP^{2+}) salts have been proposed as promising artificial cofactors of FDH to replace NADH. It was demonstrated that the reduced bipyridinium radical ($BP^{+\bullet}$) plays a role of an electron carrier for FDH in the CO_2 reduction to formic acid, while BP^{2+} cannot drive the oxidation of formic acid back to CO_2 as shown in Equation 2, this way resulting in a high reduction efficiency [17]. Also, by using the reduced 1,1′-Dimethyl-4,4′-bipyridinium (methyl viologen, $MV^{+\bullet}$), the production rate of formic acid was observed more than 20 times higher than that of NADH [18].

Similar to the process with NADH, the regeneration of artificial cofactor is essential for sustainable product generation at a low cost. Different methods have also been developed for the reduction of BP^{2+} to radical $BP^{+\bullet}$ to make the regeneration of artificial cofactor possible. For example, Secundo et al. [19] presented a visible-light-driven MV^{2+} reduction by the photosensitization of zinc tetraphenylporphyrin tetrasulfonate (ZnTPPS) and electron donor triethanolamine. Miyaji et al. [20] used chemical reagent sodium dithionite as the reducing agent of MV^{2+}. However, in these two methods, additional chemicals need to be introduced, which may harm FDH, bringing difficulties for downstream product separation. By contrast, Jayathilake et al. [21] reported a continuous electro-enzymatic conversion of CO_2 to formate by FDH with an electrochemical regeneration of $MV^{+\bullet}$, and the formate yield was found high up to 97% ± 1% over 30 hours. During the reaction, BP^{2+} acts as a stable organic salt in electrocatalysis, and only electrons are consumed. Therefore, the electrochemical method has been proposed as an efficient, inexpensive, and "clean" option to eliminate both photosensitizers and reducing agents, leading to a simple downstream product separation at a low cost.

Although an electrochemically driven enzymatic reduction of CO_2 to formic acid using FDH and the artificial cofactor $BP^{2+}/BP^{+\bullet}$ has been proposed as a promising method, the investigations in literature are so far restricted on one single bipyridinium based cofactor carrying a methyl group (MV^{2+}). It is still unclear how the performance will be when compared with the natural cofactor. For that matter of the BP^{2+} salts, besides the methyl group (weak electron-donating group), also amino and carboxylic groups are typically electron-donating and electron-withdrawing to formulate additional potential artificial cofactors [22]. These groups can affect the electron transfer from the pyridine ring to the substrate, improving the catalytic activity of FDH for CO_2 reduction. In parallel, these functional groups will also show different performances in the regeneration via electrochemical reduction. Therefore, a systematic study is needed to quantify the potential of artificial cofactors compared to NADH and understand the role of functional groups in enhancing catalytic performance. To the best of our knowledge, such research has not yet been published.

To study the performance of artificial cofactors and the effect of functional groups on electrochemically driven enzymatic CO_2 reduction to formic acid, the artificial cofactors based on the bipyridinium (BP^{2+}) salts with three different functional groups (Fig. 1), i.e., MV^{2+}, 1,1'-dicarboxyethyl-4,4'-bipyridinium bromine (DC^{2+}), and 1,1'-diaminoethyl-4,4'-bipyridinium bromine (DA^{2+}), were chosen, and their electrochemical regeneration and catalytic performance in the enzymatic reaction were systematically studied. Moreover, the enzymatic kinetics and mechanism were analyzed and discussed based on the experimental measurements and Molecular Dynamics (MD) simulations using the Umbrella sampling to gain an in-depth understanding of the effect of the functional groups in $BP^{2+}/BP^{+\bullet}$ on the reduction of CO_2 to formic acid.

2. Experimental section

2.1. Materials

Formate dehydrogenase (EC 1.2.1.2, homo-dimer, 76 kDa) from *Candida boidinii* (FDH), β-Nicotinamide adenine dinucleotide reduced form (NADH, >97 wt%), trizma base, hydrochloric acid (37%), Methyl viologen dichloride hydrate ($MVCl_2$), 4,4'-bipyridine, 3-Bromopropionic acid, 2-Bromoethylamine hydrobromide, and acetonitrile were purchased from Sigma-Aldrich. CO_2 (>99.5%) in a cylinder was purchased from AGA A/S (Sweden). MV^{2+} was purchased from Sigma-Aldrich and directly used without any further purification.

2.2. Synthesis of bipyridine derivatives

The bipyridine derivatives, other than that with MV^{2+}, were synthesized according to the literature [23]. Briefly, 1,1'-dicarboxymethyl-4,4'-bipyridinium bromine (DC^{2+}) was synthesized by heating 4,4'-bipyridine at reflux with 2 times molar equivalent of 3-Bromopropionic acid in acetonitrile (200 mL) at 90 °C for 24 h. After the reaction, the solvent was removed by rotary evaporator, and the residue was dried under vacuum overnight at 50 °C. Likewise, DA^{2+} was synthesized. The structures of the synthesized DC^{2+} and DA^{2+} were identified by ^1H NMR (Figs. S1 and S2), confirming the successful synthesis. The reduced form of artificial cofactors (with one radical in the pyridine ring) is not stable, which can easily lose one electron to generate oxidized form. The reduced form of artificial cofactors can only be formed in the electrocatalytic reaction.

2.3. Cyclic voltammetry measurements

The cyclic voltammogram of the bipyridine derivatives was measured by using a typical H-type electrochemical cell separated by a Nafion 117

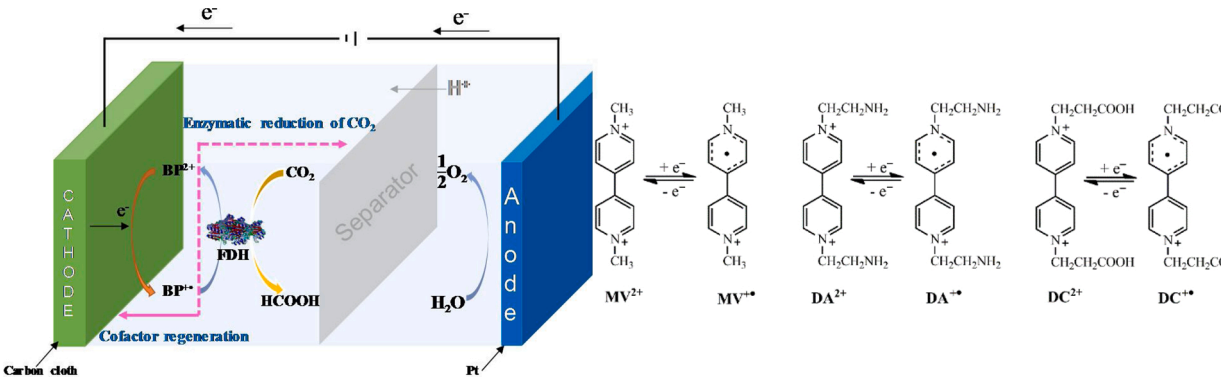

Fig. 1. (Left) schematic illustration of the bioelectrocatalytic reduction of CO_2 to formic acid, and (Right) chemical structures of the studied bipyridinium-based artificial redox cofactors.

membrane (geometrical area: 2.27 cm^2) with a three-electrode system. A carbon cloth (1 × 1 cm^2), an Ag/AgCl electrode (2 **M** KCl solution), and a platinum electrode were used as the working, reference, and counter electrodes, respectively. The working and reference electrodes were placed in the cathode chamber (10 ml) with a 100 mM phosphate buffer (pH 7.0), and the counter electrode was placed in the anode chamber (10 ml) with a 100 mM H_2SO_4 solution as the electrolyte.

2.4. CO_2 reduction to formic acid with FDH and cofactors

The reduction of CO_2 to formic acid was conducted in a typical H-type electrochemical cell described above. The sample solution in the cathode chamber was prepared with 1 mM cofactor and 0.1 mg/mL FDH (5 U/mg) in 100 mM phosphate buffer (pH 7.0). Before the experiment, the electrolyte in the cathode chamber was pre-bubbled with CO_2 (30 mL/min) for at least 30 min to achieve a CO_2-saturated solution, and the reaction was then started by applying a potential.

2.5. Measurement of enzymatic kinetics with different cofactors

The cofactors with different concentrations were prepared in CO_2-saturated 100 mM phosphate buffer with 0.1 mg/mL FDH, and the electrocatalytic conversion of CO_2 to formic acid was conducted for 10 min, whereafter the formic acid concentration was measured. Based on the detected results, the kinetic parameters were analyzed by Hanes-Woolf plots as follows:

$$\frac{[S]}{v} = \frac{[S]}{V_{max}} + \frac{K_m}{V_{max}}$$

where [S] is the substrate concentration, K_m is the Michaelis–Menten constant, and V_{max} is the maximum reaction velocity.

2.6. Analytical methods

The formate concentrations were measured by the UV-Vis spectrophotometer according to the literature [24], where sodium formate dissolved in phosphate buffer (100 mM; pH 7.0) was used for standard calibration. Solution A was prepared by dissolving 0.5 g of citric acid and 10 g of acetamide in 100 mL isopropanol, while solution B was prepared by dissolving 30 g of sodium acetate in 100 mL water. The samples (100 μL) containing formate were then mixed with 0.2 mL of solution A, 10 μL of solution B, and 0.7 mL of 100% acetic anhydride and incubated at 50 °C for 2 h with occasional mixing. Yellow color in solution was generated and measured photometrically at 515 nm.

2.7. MD simulations

It was expected that the lower free energy of the FDH + $BP^{+\bullet}$ cofactor, when associated with the CO_2 molecule, leads to a higher probability for the reduction to occur, and thus the free energy of FDH + $BP^{+\bullet}$ + CO_2 in water solution can be calculated as a function of the CO_2 position in order to identify which cofactor is more active. The calculation of free energy was based on the MD simulations using Umbrella sampling. The X-ray structure of the FDH protein was downloaded from the protein data bank (PDB ID: 5DN9) [25]. All the other molecules were built using the Avogadro software [26]. In order to perform all-atom MD simulations, the Molecular Mechanical force field parameters were generated for each artificial cofactor using the AMBER methodology and GAFF2 forcefield as the basis [27]: the geometry was minimized using the GAUSSIAN16 package [28] with the B3LYP method and the 6-31+G(d) Gaussian basis set [29]; subsequently, atomic point charges were generated using an electrostatic potential (ESP) fit [30] by the GAUSSIAN16 software. The FDH protein was simulated using the AMBER force field ff19SB [31], CO_2 was parametrized using the GAFF2 force field [27], H_3O^+ was simulated using the parameters developed by Baaden et al. [32], the ionsjc_tip3p was used for ions [33], and the TIP3P [34] model was used for water. The free energy of the system was calculated using the Umbrella sampling methodology as implemented in the GROMACS software [35].

All-atom MD simulations were performed using the GROMACS 20.4 software [36]. Three simulations were performed, one for each artificial cofactor, using the below-described protocol. The cubic periodic boundary conditions were applied, and the equations of motion of atoms were integrated with a time step of 2 fs. Van der Waals energies were calculated within a 12 Å cutoff radius. The Particle Mesh Ewald (PME) [37] method was used to calculate the electrostatic interactions with a grid spacing of 1 Å. The full electrostatic forces and non-bonded forces were calculated at each time step (2 fs). These simulations were performed in the NpT ensemble using a Parrinello-Rahman barostat for pressure control at 1 bar and the v-rescale for temperature control at 297 K. Hydrogen atom bonds were constrained to their equilibrium lengths using the LINCS algorithm [38]. Prior to dynamics, energy minimization was performed on the system. Next, the solvent was allowed to get equilibrated as the system was heated to 297 K, while the protein, cofactor, H_3O^+, and CO_2 molecules were harmonically constrained for 5 ns, followed by a simulation with the cofactor unrestrained for 5 ns. The production simulations were done using the Umbrella pulling method. Although the protein has a mirror structure with 2 active sites, only one cofactor was changed to the artificial cofactor due to the limitations of the pulling method. The cofactor was kept inside the protein by restraining it in the same position as the natural cofactor in the protein data bank structure (PDB ID: 5DN9). The CO_2 molecule was placed outside the protein and pulled inward. The initial position was chosen so that the CO_2 molecule would pass by the cofactor while being pulled. The final position of the CO_2 molecule was chosen to be one of the azide in the protein data bank structure. The CO_2 molecule was pulled towards the center of protein in 40 windows at a rate of 1 Å per window. Each

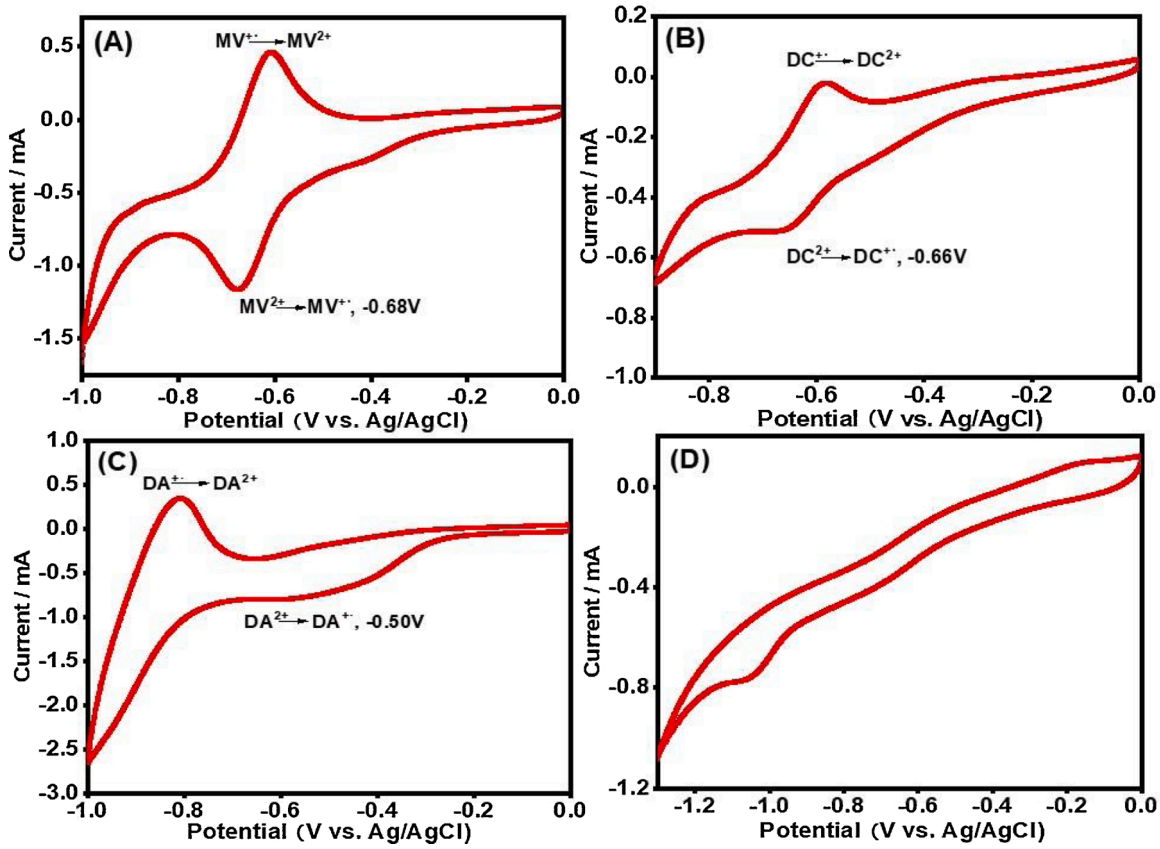

Fig. 2. CV curves of (A) MV^{2+}, (B) DC^{2+}, (C) DA^{2+}, and (D) NAD^{+}. Conditions: 1 mM cofactors in 100 mM phosphate buffer (pH 7.0) as electrolyte.

simulation window had a duration of 3 ns. The PMF graphs were obtained by using the Weighted Histogram Analysis Method (WHAM) [39].

3. Results and discussion

3.1. Electrochemical properties of cofactors

The cyclic voltammogram (CV) of different cofactors was measured in 0.1 M phosphate buffer solution from -1 to 0 V vs Ag/AgCl. The reduction peak in the CV curve stands for the reduction of the cofactor to the reduced form, and the oxidation peak indicated the cofactor is transformed from the reduced form to oxidized form. As can be seen from Fig. 2, the reduction potentials of MV^{2+}, DC^{2+}, DA^{2+}, and NAD^{+} were estimated to be -0.68, -0.66, -0.48, and -0.52 V, respectively. It meant that the reduction potential of cofactors was affected by the functional group. Of all the studied artificial cofactors, DA^{2+} showed the lowest reduction voltage, which indicated that DA^{2+} was easier to be reduced. Moreover, all these artificial cofactors presented their reversible redox peaks from -0.59 to -0.68 V, indicating that the bipyridinium salts were recyclable during the electrochemical regeneration of artificial cofactors. To further identify the reduced product (radical bipyridinium salt) and the corresponding selectivity from bipyridinium salts, the UV-Vis spectrometer was used to characterize it. As shown in Fig. S3, the artificial cofactors had a characteristic absorption at 246 nm owing to the bipyridine ring. The reduced artificial cofactors displayed only a single characteristic absorption at 605 nm, indicating that no isomers were generated during the electrocatalytic reduction, and that the reduction was highly selective. In contrast, NAD^{+} showed an irreversible feature in the CV curve, indicating the interconversion between the electro-reduced products and NAD^{+} was infeasible, which meant that NAD^{+} could not be electro-regenerated directly by the electrode. According to Wang et al., NAD dimers and isomer 1,6-NADH were easily generated with an irreversible regeneration in the electrocatalytic reduction of NAD^{+}, resulting in a permanent loss of valuable cofactor [40]. Therefore, compared to natural cofactor, artificial cofactors presented high selectivity of the reduced product and better recyclability under electrocatalysis, which are crucial for the sustainable formic acid production by electro-enzymatic conversion.

Even though the thermodynamic parameter and the equilibrium constant of enzymatic conversion of CO_2 with radical cofactor could not be used as criteria to identify the best cofactor for reaction, the difference between artificial cofactors and NADH as redox cofactor could be rationalized considering that the artificial cofactors acted only as an electron donor while NADH is both electron and proton donor. Therefore, the thermodynamic feasibility of the reaction was further investigated and analyzed. The Gibbs free energy changes (ΔG) and equilibrium constant (K) of enzymatic reduction of CO_2, including artificial cofactors and natural cofactor, were calculated according to the equations of $\Delta G = -n \cdot F \cdot E$ and $\Delta G^{\circ} = -RT\ln K$. The detailed calculations can be found in supporting information. According to the results listed in Table 1, it was found that the functional group had a great influence on ΔG and K. ΔG of the enzymatic reaction with artificial cofactors was

Table 1
The Reduction Potential of Cofactors, ΔG of CO_2 Reduction, and Equilibrium Constant K.

Cofactor	E_{red}[a] (V vs SHE)[b]	ΔG (KJ/mol)	Equilibrium constant (K)	Ratio of K_x/K_{NAD}
NAD^{+}	−0.320	38.594	1.7×10^{-7}	1
MV^{2+}	−0.483	7.140	5.6×10^{-2}	3.3×10^{5}
DC^{2+}	−0.463	10.999	1.2×10^{-2}	6.6×10^{4}
DA^{2+}	−0.393	24.507	5.1×10^{-5}	300

[a] The reduction potential.
[b] $E_{SHE} = E_{Ag}/AgCl + E_{Ag}/AgCl$ vs NHE (0.197).

lower than that with natural cofactor NADH, indicating that the artificial cofactors possessed a more favorable thermodynamic driving force. On the other hand, the equilibrium constant K of enzymatic reaction with the natural cofactor (NADH) was the lowest (1.7×10^{-7}), indicating a low conversion of CO_2 caused by the oxidation of formate. This is consistent with other observations; for example, as reported, to shift the reaction towards formate with NADH, at least two orders of magnitude in concentration for the substrates (NADH or CO_2) were required, compared to the concentration of formate.[21] By contrast, the artificial cofactors presented a much higher value of equilibrium constant K, and MV^{2+}, in particular, showed the highest value of 5.6×10^{-2}, which was expected to realize an increased conversion of CO_2. Therefore, the artificial cofactors exhibited a better catalytic performance in terms of thermodynamics.

3.2. Conversion of CO_2 to formic acid with different cofactors

To evaluate the reduction performance, the enzymatic reduction of CO_2 to formic acid using FDH with the reduced cofactor $MV^{+\bullet}$, $DC^{+\bullet}$, or $DA^{+\bullet}$, was carried out in their reduction peak potential vs. Ag/AgCl for 1 h. NADH was also studied for comparison. As shown in Fig. 3, the concentrations of formic acid, at 60 minutes, were 1.3, 3.5, 2.0, and 0.1 mM, for those with $MV^{+\bullet}$, $DA^{+\bullet}$, $DC^{+\bullet}$, and NADH, respectively. In case of NADH, the formic acid concentration showed the lowest value, since NAD^+ could not efficiently be reduced (around 1%) under electrocatalysis when using carbon cloth as the electrode. This result agreed with the CV of NAD^+ in Fig. 2, where irreversible redox peaks were observed. Therefore, there is poor interconversion between NAD^+ and NADH and thus poor performance on the electroreduction of NAD^+ to NADH. Differently, the artificial cofactors presented a much better performance on the stability, lower request for electrode, and were effective on CO_2 conversion. Particularly, the formic acid concentration for the system with $DA^{+\bullet}$ was about 35 times higher than that of natural cofactor NADH. Moreover, compared to values of reduction potential for artificial cofactors listed in Table 1, the concentration of formic acid increased with increase of reduction potential, which meant that the reduction of CO_2 to formic acid did depend on the functional group of bipyridinium salts.

To clarify why artificial cofactors could enhance formic acid production, the formic acid oxidation to CO_2 catalyzed by FDH with the cofactors of MV^{2+}, DA^{2+}, DC^{2+}, or NAD^+ was also conducted. It was shown that, after the reaction, no reduced form of artificial cofactors was detected. This observation indicated that the excellent reduction performance of CO_2 to formic acid in the presence of artificial cofactors was attributed to the suppression of reversible reaction. In contrast, when NAD^+ served as the cofactor, a quite fast oxidation rate of formic acid was observed. As reported in the literature [41], the oxidation rate of formic acid was 30 times higher than that of the CO_2 reduction catalyzed by FDH using the natural redox cofactor $NADH/NAD^+$. As a result, the formation of formic acid reached equilibrium quickly but with a very low concentration. According to the above results, the bipyridinium salts are promising cofactors for the enzymatic reduction of CO_2, and they were further investigated from the kinetics aspect in the following section.

3.3. Kinetic analysis of enzymatic reaction

To clarify how the functional groups of bipyridinium salts influence the conversion of CO_2, the kinetics studies of enzymatic reaction in the presence of different cofactors with the same concentration (0.1 mg/ml FDH) were carried out. Fig. 4 depicts the relationship between the production rate of formic acid and the concentration of artificial cofactors. A steep increase in the production rate of formic acid was observed with increasing the concentration of reduced cofactors up to nearly 10 mM, while the further increase in the cofactor concentration (i.e., beyond ~10 mM) only led to a slight increase in the production rate. The experimental data determined in this work was further described with the Michaelis–Menten equation, as illustrated in Fig. 4, showing that the experimental results followed the Michaelis-Menten kinetics. This indicated that the bipyridinium salts served as the coenzyme of FDH. It has been reported that the FDH activity was inhibited when the concentration of NADH was higher than 0.45 mM, and the formic acid concentration only reached the highest value at 0.45 mM and decreased when the concentration of NADH was either lower or higher than 0.45 mM [42–43]. However, such phenomenon was not observed, i.e., the FDH activity was not restricted by increasing the concentration of artificial cofactors, which was another advantage of using artificial cofactor for the enzymatic conversion of CO_2.

Next, the Hanes-Woolf equation [44] was used to describe the enzymatic kinetics of CO_2 reduction to formic acid, and the parameters of enzymatic kinetics, i.e., Michaelis constant (K_m), maximum velocity (V_{max}), catalytic constant (k_{cat}), and catalytic efficiency (k_{cat}/K_m), were calculated from the determined experimental data. The obtained parameters are listed in Table 2. The constant K_m refers to the substrate concentration at which the reaction rate is half of the maximum velocity (V_{max}), reflecting the affinity strength between the enzyme and substrate. As a result, the enzyme with a lower K_m indicated a stronger

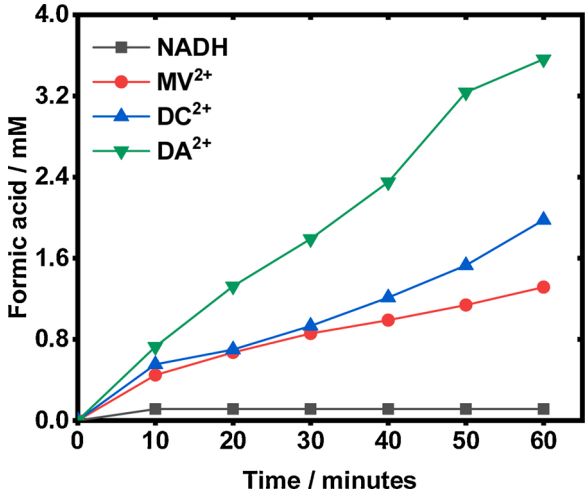

Fig. 3. The concentration of formic acid as a function of time with 1 mM different cofactors at their corresponding reduction peak potential vs. Ag/AgCl in 100 mM phosphate buffer (pH 7) as electrolyte.

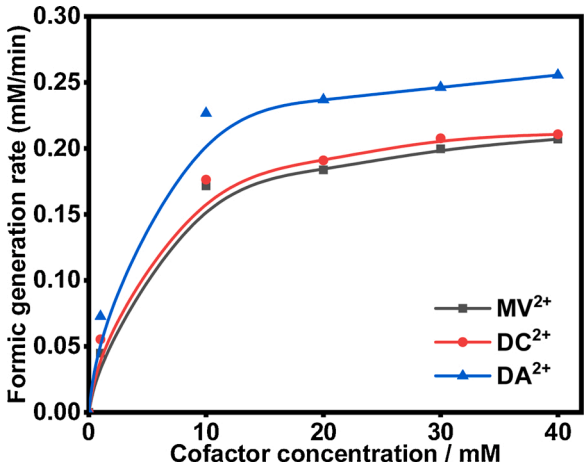

Fig. 4. Relationship between the initial formic acid production rate and the concentration of cofactors. Symbols: experimental results; Curves: fitted to the Michaelis-Menten equation.

Table 2
Kinetic Parameters for the Reduction of CO_2 to Formic Acid with Different co-factors and FDH.

Cofactor	K_m (mM)	V_{max} (mM•min^{-1})	k_{cat} (min^{-1})	k_{cat}/K_m (mM^{-1} min^{-1})
$DA^{+\bullet}$	2.782	0.276	0.448	0.161
$DC^{+\bullet}$	3.101	0.227	0.256	0.082
$MV^{+\bullet}$	4.133	0.230	0.166	0.040
NADH	50	0.002	0.013	0.0003

affinity and resulted in a higher rate and conversion of reaction. As K_m values decreased in the order of K_m(NADH) > K_m($MV^{+\bullet}$) > K_m($DC^{+\bullet}$) > K_m($DA^{+\bullet}$), their affinity with FDH increased in the order of NADH < $MV^{+\bullet}$ < $DC^{+\bullet}$ < $DA^{+\bullet}$, and the affinity between FDH and $DA^{+\bullet}$ was the strongest. Consequently, $DA^{+\bullet}$ with the strongest affinity (lowest K_m) displayed the best catalytic performance. Likewise, catalytic constant k_{cat} increased in the order of k_{cat}(NADH) < k_{cat}($MV^{+\bullet}$) < k_{cat}($DC^{+\bullet}$) < k_{cat}($DA^{+\bullet}$), being consistent with the order of affinity. Subsequently, the calculated catalytic efficiency (k_{cat}/K_m) increased with the same order of k_{cat} but showed much bigger values, and the catalytic efficiency of $DA^{+\bullet}$ was around 536 times higher than that of NADH. Therefore, it was demonstrated that the performance of artificial cofactors in the reaction was affected by the functional groups, and $DA^{+\bullet}$ with the highest affinity had the best catalytic efficiency.

As the pH of the medium drives the molar ratio of CO_2 to HCO_3- and is thus sensitive to CO_2 conversion, enzymatic reaction with artificial cofactor DA^{2+} was conducted in the pH ranging from 6.5 to 8.5 and the potential relationship between the molar ratio of CO_2 to HCO_3- and CO_2 conversion was explored. As shown in Fig. S4A, the conversion rate reaches the highest value at pH 7, which is consistent with reported results when using a natural cofactor [45]. Meanwhile, the molar ratio of CO_2 to HCO_3- was analyzed according to the Bjerrum plot illustrated in Figure S4B [46]. The analysis shows that, with increasing pH from 6.5 to 8, CO_2 concentration decreases while that for HCO_3- increases, indicating that CO_2 is continuously transformed into HCO_3- and achieves complete transformation at pH 8. Also, the highest conversion of CO_2 was obtained at pH 7, indicating both CO_2 and HCO_3- might serve as substrates to FDH, and the FDH activity plays a decisive role on CO_2 conversion within this pH range. While, the further increase of pH from 8 will decrease HCO_3- concentration, i.e., HCO_3- will convert to CO_3^{2-}, resulting in the decrease of the substrate concentration for FDH and thus lowering the conversion of CO_2.

To evaluate the potential of electrochemically driven CO_2 reduction to formic acid with FDH and the bipyridinium salt as a cofactor, the formation rate of formic acid obtained in this work was compared with the enzymatic CO_2 reduction processes driven by the visible-light or reducing agents reported in the literature (Table 3). The comparison clearly revealed that the enzymatic reduction of CO_2 with electrochemically-reduced cofactors provided a higher formic acid production compared with the dithionite-reduced and visible-light-reduced cofactors. Additionally, in the process of visible-light-reduced cofactor, the system typically contained photosensitizer, electron mediator, electron donor, enzymes, and coenzymes [16]. Such a complex system would usually bring the problems of the downstream product separation. Furthermore, the enzyme activity was sensitive to temperature, while the system would suffer from temperature increases under the light irradiation in the long run, leading to a decrease in enzyme activity. When using dithionite for the reduction of the cofactor, the strong reductant was potentially harmful to the enzyme activity, and the addition of byproduct (reductant) to the reaction mixture is also not desirable for the downstream product separation. The direct electrocatalytic reduction of artificial cofactor was relatively "clean", and only electrons were consumed. Therefore, electrochemically driven enzymatic CO_2 reduction is an attractive candidate for an efficient conversion of CO_2 to formic acid, due to the excellent formic acid production and more simple operation.

Table 3
Comparison of the Formic Acid Formation Rate with Other Visible-light or Reducing Agents Driven CO2 Reduction to Formic Acid.

Cofactor	Incubation time	Formic acid concentration (mM)	Formic acid formation rate (mM/h)[i]	Ref.
Electrochemically-reduced DA^{2+}	1 h	3.5	3.5	This work
Electrochemically-reduced DC^{2+}	1 h	2.0	2.0	This work
Electrochemically-reduced MV^{2+}	1 h	1.3	1.3	This work
Dithionite-reduced MV^{2+}	1 h	1.9	1.9	[18]
Dithionite-reduced $MCABP^{2+}$[a]	10 min	0.035	0.21	[47]
Dithionite-reduced $DCABP^{2+}$[b]	10 min	0.0248	0.15	[47]
Dithionite-reduced $NEMBP^{2+}$[c]	10 min	0.005	0.03	[47]
Visible-light-reduced MV^{2+}	1 h	~ 0.06	~ 0.06	[48]
Visible-light-reduced MV^{2+}	3 h	0.105	0.035	[49]
Visible-light-reduced CV^{2+}[d]	3 h	0.149	0.050	[49]
Visible-light-reduced C_b MV^{2+}[e]	3 h	0.172	0.058	[49]
Visible-light-reduced DA^{2+}	3 h	0.120	0.040	[50]
Visible-light-reduced AMV^{2+}[f]	3 h	0.130	0.043	[50]
Visible-light-reduced CMV^{2+}[g]	3 h	0.085	0.028	[50]
Visible-light-reduced DCV^{2+}[h]	3 h	0.083	0.028	[50]

[a] $MCABP^{2+}$: 1-carbamoylmethyl-1'-methyl-4,4'-bipyridinium salt.
[b] $DCABP^{2+}$: 1,1'-dicarbamoylmethyl-4,4'-bipyridinium salt.
[c] $NEMBP^{2+}$: 1-nicotinamidethyl-1'-methyl-4,4'-bipyridinium salt.
[d] CV^{2+}: 1,1'-dicarbamoylmethyl-4,4'-bipyridinium salt.
[e] C_b MV^{2+}: 1-carbamoylmethyl-1'-methyl-4,4'-bipyridinium salt.
[f] AMV^{2+}: 1-amino-1'-methyl-4,4'-bipyridinium salt.
[g] CMV^{2+}: 1-carboxyl-1'-methyl-4,4'-bipyridinium salt.
[h] DCV^{2+}: 1,1'-dicarboxyl-4,4'-bipyridinium salt.
[i] Formic acid formation rate equal to formic acid concentration divided by incubation time.

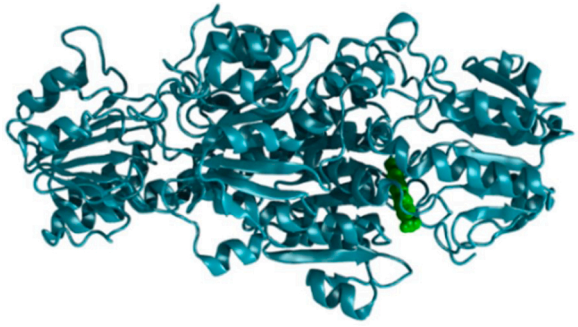

Fig. 5. Structure of the FDH protein with the natural cofactor replaced with the artificial $MV^{+\bullet}$ cofactor. The protein is represented in cartoon style in teal, and the $MV^{+\bullet}$ molecule is represented in green as VdW spheres.

3.4. CO_2 affinity investigation by MD simulations

To explain the outstanding performance of artificial cofactors, the active site of FDH, replacing natural cofactor with artificial cofactors, was investigated by MD simulations. In order to verify the affinity of the CO_2 molecule to each cofactor in the active site of enzymes, the Potential of Mean Force (PMF) was calculated using the protocol described in

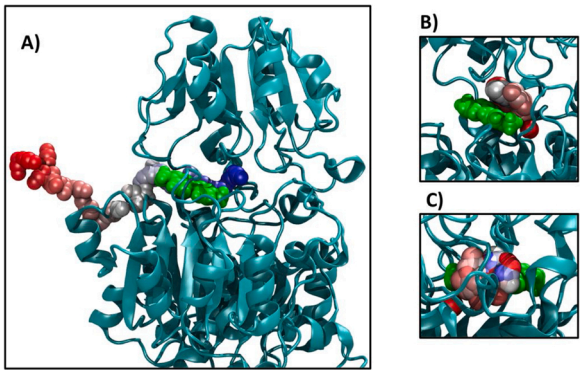

Fig. 6. A) Representation of the position of the CO_2 molecule at the start of each Umbrella sampling window. **B)** and **C)** show the movement of the CO_2 molecule in a window where it is close to the cofactor. The $MV^{+\bullet}$ cofactor is depicted in green as VdW spheres, the protein is depicted in cartoon style in teal, and the CO_2 molecules are depicted as a chain of VdW spheres that change colors from red at the beginning of the trajectory, to white and to blue at the end.

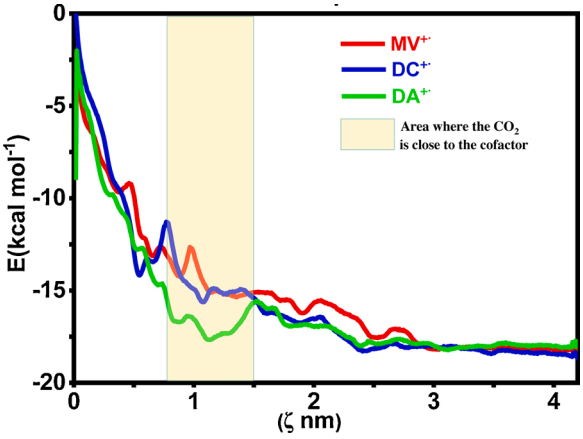

Fig. 7. Plots of the changes in free energy as the CO_2 molecules move from the outside to the inside of the protein in the presence of 3 artificial cofactors.

Section 2.7. Fig. 5 depicts the structure of the protein with the NAD^+ cofactor replaced with the artificial cofactor $MV^{+\bullet}$.

Fig. 6A depicts the position of the CO_2 molecule at the start of each Umbrella sampling window for the simulations with the $MV^{+\bullet}$ cofactor. The CO_2 molecule was pulled from the outside of the protein to the inside at a rate of 1 Å/window. For the $DA^{+\bullet}$ and $CA^{+\bullet}$ cofactors, the same initial structure file was used for each window, i.e., only replacing the $MV^{+\bullet}$ cofactor with the other one. Fig. 6B and C depict the trajectory of the CO_2 molecule in window 35/40 when it is close to the $MV^{+\bullet}$ cofactor. As we can see, the Umbrella restraint allows the CO_2 molecule to explore space around the cofactor and find the most favorable position.

Using WHAM, PMF of the systems for all of the artificial cofactors was calculated. As it can be seen in Fig. 7, the curves are almost identical for all 3 cases, except in the region where the CO_2 molecule is in contact with the cofactor that is highlighted in yellow in the figure. In this region, we can see that the free energy is lower when the $DA^{+\bullet}$ cofactor is presented. This points to a better affinity of the CO_2 molecule to the $DA^{+\bullet}$ cofactor, which could explain why this cofactor has a better rate to reduce CO_2.

Note that, in water, CO_2 is in equilibrium with HCO_3-, and the latter is dominant in bulk at physiological pH. However, which of these two forms is favored inside the active site cannot be predicted. According to the report, the conversion of CO_2 catalyzed by FDH was enhanced by adding carbonic anhydrase (CA) [51], where CA has a function of accelerating the hydration of CO_2 to HCO_3-. Furthermore, the authors Miyaji et al. [20] also suggested that HCO_3- was the substrate of FDH from their experimental results. On the contrary, the authors Marta et al. [52] declared that FDH reduced CO_2 rather than HCO_3^- as verified by the electrochemical analysis. In any case, the artificial cofactor $DA^{2+}/DA^{+\bullet}$ has the highest affinity in this study, and MD shows a higher affinity of CO_2 molecule to $DA^{+\bullet}$ when this form was used as the substrate for reaction. Since this artificial cofactor is positively charged, we can expect that HCO_3- as the substrate should have an even higher affinity to $DA^{+\bullet}$, owing to electrostatic interaction. Therefore, an enhanced affinity of CO_2 to $DA^{+\bullet}$ accounted for the improvement of product concentration.

4. Conclusions

In this work, three artificial cofactors, MV^{2+}, DA^{2+}, and DC^{2+} were synthesized and used for the enzymatic CO_2 reduction to formic acid. All of the electrochemically-reduced bipyridinium salts showed a superior reduction performance compared with the natural cofactor NADH due to the suppression of reverse oxidation reaction. Among the studied cofactors, DA^{2+}, i.e., the one with the amino group, exhibited the lowest reduction potential, highest formic acid concentration, and fastest reaction kinetics. The k_{cat}/K_m value of DA^{2+} was 2, 4, and 536 times higher than those of DC^{2+}, MV^{2+}, and NADH, respectively. Experimental results demonstrated the highest affinity between $DA^{+\bullet}$ and FDH (substrate-FDH), and simulation results proved that CO_2 affinity is the highest for the $DA^{+\bullet}$ cofactor (substrate-substrate), which both explained the highest yield of product at the presence of $DA^{+\bullet}$. By comparing with the dithionite-reduced and visible-light-reduced artificial cofactors, electrochemically-reduced cofactors showed advantages for enzymatic reduction, implying the high potential of electrochemically driven enzymatic reduction of CO_2 to formic acid.

CRediT authorship contribution statement

Zhibo Zhang: Methodology, Formal analysis, Visualization, Writing - original draft, Writing - review & editing. **Tudor Vasiliu**: simulation investigation, writing & editing. **Fangfang Li**: writing & editing. **Aatto Laaksonen**: Conceptualization, writing & editing. **Francesca Mocci**: Conceptualization, Writing - review & editing. **Xiaoyan Ji**: Conceptualization, Supervision, Writing - original draft, Writing - review & editing.

Declaration of Competing Interest

The authors report no declarations of interest.

Acknowledgment

Z. Zhang and X. Ji thank the financial support from the Kempe foundation in Sweden. F. Li and X. Ji acknowledge the financial support from the Swedish Energy Agency (P47500-1). A. Laaksonen acknowledges the Swedish Research Council for financial support, and partial support from Ministry of Research and Innovation of Romania (CNCS - UEFISCDI, project number PN-III-P4-ID-PCCF-2016-0050, within PNCDI III). F. Mocci acknowledges financial support from Progetto Fondazione di Sardegna (Grant CUP: F72F20000230007) and Regione Autonoma della Sardegna (RASSR81788-2017).

Appendix A. Supplementary data

Supplementary material related to this article can be found, in the online version, at doi:https://doi.org/10.1016/j.jcou.2021.101679.

References

[1] Y.Y. Lee, H.S. Jung, Y.T. Kang, A review: Effect of nanostructures on photocatalytic co2 conversion over metal oxides and compound semiconductors, J Co2 Util 20 (2017) 163–177.
[2] F. Li, F. Mocci, X. Zhang, X. Ji, A. Laaksonen, Ionic liquids for co2 electrochemical reduction, Chinese Journal of Chemical Engineering (2020).
[3] D.A. Bulushev, J.R.H. Ross, Towards sustainable production of formic acid, Chemsuschem 11 (5) (2018) 821–836.
[4] P. Upadhyay, V. Srivastava, Carbon sequestration: Hydrogenation of co2 to formic acid, Present Environment and Sustainable Development 10 (2) (2016) 13–34.
[5] A. Dibenedetto, P. Stufano, W. Macyk, T. Baran, C. Fragale, M. Costa, M. Aresta, Hybrid technologies for an enhanced carbon recycling based on the enzymatic reduction of co2 to methanol in water: Chemical and photochemical nadh regeneration, Chemsuschem 5 (2) (2012) 373–378.
[6] D.W. Du, R. Lan, J. Humphreys, S.W. Tao, Progress in inorganic cathode catalysts for electrochemical conversion of carbon dioxide into formate or formic acid, Journal of Applied Electrochemistry 47 (6) (2017) 661–678.
[7] Y. Amao, Formate dehydrogenase for co2 utilization and its application, J Co2 Util 26 (2018) 623–641.
[8] C. Federsel, C. Ziebart, R. Jackstell, W. Baumann, M. Beller, Catalytic hydrogenation of carbon dioxide and bicarbonates with a well-defined cobalt dihydrogen complex, Chemistry-a European Journal 18 (1) (2012) 72–75.
[9] N.V.D. Long, J. Lee, K.K. Koo, P. Luis, M. Lee, Recent progress and novel applications in enzymatic conversion of carbon dioxide, Energies 10 (4) (2017).
[10] M.W. Yuan, M.J. Kummer, S.D. Minteer, Strategies for bioelectrochemical co2 reduction, Chemistry-a European Journal 25 (63) (2019) 14258–14266.
[11] J.F. Shi, Y.J. Jiang, Z.Y. Jiang, X.Y. Wang, X.L. Wang, S.H. Zhang, P.P. Han, C. Yang, Enzymatic conversion of carbon dioxide, Chemical Society Reviews 44 (17) (2015) 5981–6000.
[12] H. Choe, J.C. Joo, D.H. Cho, M.H. Kim, S.H. Lee, K.D. Jung, Y.H. Kim, Efficient co2-reducing activity of nad-dependent formate dehydrogenase from thiobacillus sp knk65ma for formate production from co2 gas, Plos One 9 (7) (2014).
[13] Z.B. Zhang, J. Muschiol, Y.H. Huang, S.B. Sigurdardottir, N. von Solms, A. E. Daugaard, J. Wei, J.Q. Luo, B.H. Xu, S.J. Zhang, M. Pinelo, Efficient ionic liquid-based platform for multi-enzymatic conversion of carbon dioxide to methanol, Green Chemistry 20 (18) (2018) 4339–4348.
[14] M. Aresta, A. Dibenedetto, T. Baran, A. Angelini, P. Labuz, W. Macyk, An integrated photocatalytic/enzymatic system for the reduction of co2 to methanol in bioglycerol-water, Beilstein J Org Chem 10 (2014) 2556–2565.
[15] Z. Zhang, J. Li, M. Ji, Y. Liu, N. Wang, X. Zhang, S. Zhang, X. Ji, Encapsulation of multiple enzymes in a metal–organic framework with enhanced electro-enzymatic reduction of co2 to methanol, Green Chemistry 23 (6) (2021) 2362–2371.
[16] S.K. Kuk, R.K. Singh, D.H. Nam, R. Singh, J.K. Lee, C.B. Park, Photoelectrochemical reduction of carbon dioxide to methanol through a highly efficient enzyme cascade, Angewandte Chemie-International Edition 56 (14) (2017) 3827–3832.
[17] S. Ikeyama, Y. Amao, Novel artificial coenzyme based on the viologen derivative for co2 reduction biocatalyst formate dehydrogenase, Chemistry Letters 45 (11) (2016) 1259–1261.
[18] Y. Amao, S. Ikeyama, Discovery of the reduced form of methylviologen activating formate dehydrogenase in the catalytic conversion of carbon dioxide to formic acid, Chemistry Letters 44 (9) (2015) 1182–1184.
[19] F. Secundo, Y. Amao, Visible-light-driven co2 reduction to formate with a system of water-soluble zinc porphyrin and formate dehydrogenase in ionic liquid/aqueous media, Rsc Advances 10 (69) (2020) 42354–42362.
[20] A. Miyaji, Y. Amao, How does methylviologen cation radical supply two electrons to the formate dehydrogenase in the catalytic reduction process of co(2)to formate? Physical Chemistry Chemical Physics 22 (33) (2020) 18595–18605.
[21] B.S. Jayathilake, S. Bhattacharya, N. Vaidehi, S.R. Narayanan, Efficient and selective electrochemically driven enzyme-catalyzed reduction of carbon dioxide to formate using formate dehydrogenase and an artificial cofactor, Accounts of Chemical Research 52 (3) (2019) 676–685.
[22] A.P. Cismesia, G.R. Nicholls, N.C. Polfer, Amine vs. Carboxylic acid protonation in ortho-, meta-, and para-aminobenzoic acid: An irmpd spectroscopy study, J Mol Spectrosc 332 (2017) 79–85.
[23] S. Ikeyama, Y. Amao, An artificial co-enzyme based on the viologen skeleton for highly efficient co2 reduction to formic acid with formate dehydrogenase, Chemcatchem 9 (5) (2017) 833–838.
[24] R.K. Singh, R. Singh, D. Sivakumar, S. Kondaveeti, T. Kim, J.L. Li, B.H. Sung, B. K. Cho, D.R. Kim, S.C. Kim, V.C. Kalia, Y.H.P.J. Zhang, H.M. Zhao, Y.C. Kang, J. K. Lee, Insights into cell-free conversion of co2 to chemicals by a multienzyme cascade reaction, Acs Catalysis 8 (12) (2018) 11085–11093.
[25] Q. Guo, L. Gakhar, K. Wickersham, K. Francis, A. Vardi-Kilshtain, D.T. Major, C. M. Cheatum, A. Kohen, Structural and kinetic studies of formate dehydrogenase from candida boidinii, Biochemistry-Us 55 (19) (2016) 2760–2771.
[26] M.D. Hanwell, D.E. Curtis, D.C. Lonie, T. Vandermeersch, E. Zurek, G.R. Hutchison, Avogadro: An advanced semantic chemical editor, visualization, and analysis platform, J Cheminformatics 4 (2012).
[27] J.M. Wang, R.M. Wolf, J.W. Caldwell, P.A. Kollman, D.A. Case, Development and testing of a general amber force field, J Comput Chem 25 (9) (2004) 1157–1174.
[28] M.J. Frisch, G.W. Trucks, H.B. Schlegel, G.E. Scuseria, M.A. Robb, J.R. Cheeseman, G. Scalmani, V. Barone, G.A. Petersson, H. Nakatsuji, X. Li, M. Caricato, A. V. Marenich, J. Bloino, B.G. Janesko, R. Gomperts, B. Mennucci, H.P. Hratchian, J. V. Ortiz, A.F. Izmaylov, J.L. Sonnenberg, F. Williams; Ding, F. Lipparini, F. Egidi, J. Goings, B. Peng, A. Petrone, T. Henderson, D. Ranasinghe, V.G. Zakrzewski, J. Gao, N. Rega, G. Zheng, W. Liang, M. Hada, M. Ehara, K. Toyota, R. Fukuda, J. Hasegawa, M. Ishida, T. Nakajima, Y. Honda, O. Kitao, H. Nakai, T. Vreven, K. Throssell, J.A. Montgomery Jr., J.E. Peralta, F. Ogliaro, M.J. Bearpark, J. J. Heyd, E.N. Brothers, K.N. Kudin, V.N. Staroverov, T.A. Keith, R. Kobayashi, J. Normand, K. Raghavachari, A.P. Rendell, J.C. Burant, S.S. Iyengar, J. Tomasi, M. Cossi, J.M. Millam, M. Klene, C. Adamo, R. Cammi, J.W. Ochterski, R.L. Martin, K. Morokuma, O. Farkas, J.B. Foresman, D.J. Fox, Gaussian 16 rev. C.01, Wallingford, CT, 2016.
[29] W.J. Hehre, R. Ditchfield, J.A. Pople, Self—consistent molecular orbital methods. Xii. Further extensions of gaussian—type basis sets for use in molecular orbital studies of organic molecules, The Journal of Chemical Physics 56 (5) (1972) 2257–2261.
[30] C.I. Bayly, P. Cieplak, W.D. Cornell, P.A. Kollman, A well-behaved electrostatic potential based method using charge restraints for deriving atomic charges - the resp model, Journal of Physical Chemistry 97 (40) (1993) 10269–10280.
[31] C. Tian, K. Kasavajhala, K.A.A. Belfon, L. Raguette, H. Huang, A.N. Migues, J. Bickel, Y.Z. Wang, J. Pincay, Q. Wu, C. Simmerling, Ff19sb: Amino-acid-specific protein backbone parameters trained against quantum mechanics energy surfaces in solution, J Chem Theory Comput 16 (1) (2020) 528–552.
[32] M. Baaden, M. Burgard, G. Wipff, Tbp at the water-oil interface: The effect of tbp concentration and water acidity investigated by molecular dynamics simulations, J Phys Chem B 105 (45) (2001) 11131–11141.
[33] I.S. Joung, T.E. Cheatham, Molecular dynamics simulations of the dynamic and energetic properties of alkali and halide ions using water-model-specific ion parameters, J Phys Chem B 113 (40) (2009) 13279–13290.
[34] P. Mark, L. Nilsson, Structure and dynamics of the tip3p, spc, and spc/e water models at 298 k, J Phys Chem A 105 (43) (2001) 9954–9960.
[35] G.M. Torrie, J.P. Valleau, Non-physical sampling distributions in monte-carlo free-energy estimation - umbrella sampling, J Comput Phys 23 (2) (1977) 187–199.
[36] D. Van der Spoel, E. Lindahl, B. Hess, G. Groenhof, A.E. Mark, H.J.C. Berendsen, Gromacs: Fast, flexible, and free, J Comput Chem 26 (16) (2005) 1701–1718.
[37] U. Essmann, L. Perera, M.L. Berkowitz, T. Darden, H. Lee, L.G. Pedersen, A smooth particle mesh ewald method, J Chem Phys 103 (19) (1995) 8577–8593.
[38] B. Hess, H. Bekker, H.J.C. Berendsen, J.G.E.M. Fraaije, Lincs: A linear constraint solver for molecular simulations, J Comput Chem 18 (12) (1997) 1463–1472.
[39] S. Kumar, D. Bouzida, R.H. Swendsen, P.A. Kollman, J.M. Rosenberg, The weighted histogram analysis method for free-energy calculations on biomolecules .1. The method, J Comput Chem 13 (8) (1992) 1011–1021.
[40] Xiaodong Wang, Tony Saba, Humphrey H.P. Yiu, Russell F. Howe, James A. Anderson, Jiafu Shi, Cofactor nad(p)h regeneration inspired by heterogeneous pathways, chem 2 (2017) 621–654.
[41] U. Ruschig, U. Muller, P. Willnow, T. Hopner, Co2 reduction to formate by nadh catalyzed by formate dehydrogenase from pseudomonas-oxalaticus, European Journal of Biochemistry 70 (2) (1976) 325–330.
[42] R. Barin, D. Biria, S. Rashid-Nadimi, M.A. Asadollahi, Enzymatic co2 reduction to formate by formate dehydrogenase from candida boidinii coupling with direct electrochemical regeneration of nadh, J Co2 Util 28 (2018) 117–125.
[43] S. Kim, M.K. Kim, S.H. Lee, S. Yoon, K.D. Jung, Conversion of co2 to formate in an electroenzymatic cell using candida boidinii formate dehydrogenase, J Mol Catal B-Enzym 102 (2014) 9–15.
[44] H. Lineweaver, D. Burk, The determination of enzyme dissociation constants, J Am Chem Soc 56 (3) (1934) 658–666.
[45] Z.B. Zhang, B.H. Xu, J.Q. Luo, N. Von Solms, H.Y. He, Y.Q. Zhang, M. Pinelo, S. J. Zhang, Ionic liquids as bifunctional cosolvents enhanced co2 conversion catalysed by nadh-dependent formate dehydrogenase, Catalysts 8 (8) (2018).
[46] C.B. Andersen, Understanding carbonate equilibria by measuring alkalinity in experimental and natural systems, Journal of Geoscience Education 50 (2002) 357. -36.
[47] A. Miyaji, Y. Amao, Artificial co-enzyme based on carbamoyl-modified viologen derivative cation radical for formate dehydrogenase in the catalytic co2 reduction to formate, New Journal of Chemistry 44 (43) (2020) 18803–18812.
[48] Y. Amao, R. Abe, S. Shiotani, Effect of chemical structure of bipyridinium salts as electron carrier on the visible-light induced conversion of co2 to formic acid with the system consisting of water-soluble zinc porphyrin and formate dehydrogenase, J Photoch Photobio A 313 (2015) 149–153.
[49] S. Ikeyama, T. Katagiri, Y. Amao, The improvement of formic acid production from co2 with visible-light energy and formate dehydrogenase by the function of the viologen derivative with carbamoylmethyl group as an electron carrier, J Photoch Photobio A 358 (2018) 362–367.
[50] S. Ikeyama, Y. Amao, The effect of the functional ionic group of the viologen derivative on visible-light driven co2 reduction to formic acid with the system consisting of water-soluble zinc porphyrin and formate dehydrogenase, Photochemical & Photobiological Sciences 17 (1) (2018) 60–68.
[51] X. Ji, Z. Su, P. Wang, G. Ma, S. Zhang, Tethering of nicotinamide adenine dinucleotide inside hollow nanofibers for high-yield synthesis of methanol from carbon dioxide catalyzed by coencapsulated multienzymes, Acs Nano 9 (4) (2015) 4600–4610.
[52] Marta Meneghello, A.R. Oliveira, Aurore Jacq-Bailly, Inês A.C. Pereira, Christophe Léger, Vincent Fourmond, Formate dehydrogenases reduce co2 rather than hco3−: An electrochemical demonstration, Angew Chem Int Edit 60 (2021) 1–5.